A Balun-Integrated On-Chip Differential Pad for Full/Multi-Band mmWave/THz Measurements

J. Grzyb[1], M. Andree, P. Hillger, T. Bücher, U. R. Pfeiffer[2]
University of Wuppertal, Wuppertal, Germany
[1]grzyb@uni-wuppertal.de, [2]ullrich.pfeiffer@uni-wuppertal.de

***Abstract* — A set of balun-integrated 100/300 GHz differential on-chip pads for broadband characterization (small/large-signal) of active circuits fabricated in SiGe HBT technology is presented. A general theory of asymmetric coupled-lines in inhomogeneous medium was applied to design a Marchand-like balun consisting of multiple sub-λ/4 long nonuniformly-sized line sections with a close-proximity ground-plane to compensate for the frequency-dependent pad impedance.**

***Keywords* — Marchand balun, on-chip differential pad, mmWave, THz measurement.**

I. Introduction

Differential operation is commonly applied at mmWave and THz frequencies to active circuits. Their accurate characterization, both small- as well as large-signal, is essential and challenging at the same time at such high frequencies. The pure-mode VNAs or the 4-port VNAs with the multi-mode TRL calibration technique [1] are here practically unavailable. Therefore, de-embedding the impact of any error network between the calibration reference plane and the differential DUT may become a tedious task with the classical 2-port VNA system. With the availability of a broadband balun-integrated on-chip differential pad with a low return loss at both balanced and unbalanced ports, the measurements can be greatly simplified after the initial calibration with a standard calibration substrate. A systematic analysis with the corresponding design approach and relevant comparison data of such pads operating at near-THz frequencies is not fully addressed in the literature and defines the scope of this paper.

II. On-chip pad

Two similar single-ended 50 Ω pads (see Fig. 2) were dimensioned in a 7-layer BEOL SiGe HBT technology from IHP for on-chip probing around 100/300 GHz. The pad pitch and the signal pad width are 200 μm and 50 μm, respectively. The transmission path between the probe ('Probe1') and output ('In') ports includes a 25 μm long 50 Ω microstrip line on TM2 and a via transition to the balun reference plane on TM1. The simulated (Ansys HFSS) Smith chart corresponding to both pads is shown in Fig. 1. The excitation at the probe side is defined with 2 lumped ports (Probe 1/Probe 1') between the signal and the ground pads driven in-phase, which mimics the probe-tip locations. Up to around 160 GHz, the pad can be well approximated by a low-pass LC network (L_{pad}=21.5 pH, C_{pad}=21 fF). Toward 300 GHz, the pad output impedance scales down to 20–25 Ω. To facilitate broadband 100 Ω differential measurements, the nominal 50–to–100 Ω balun needs to absorb the pad low-pass characteristics in the first design case (< 160 GHz), whereas for operation in WR3 band, an additional 25–100 Ω impedance transformation needs to be provided, thus challenging the operation bandwidth.

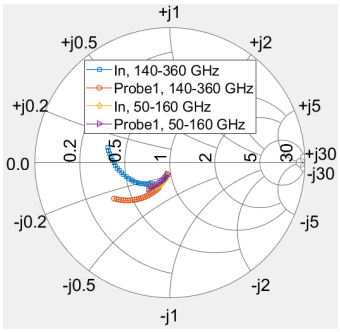

Fig. 1. Simulated Smith chart of the 100 GHz and 300 GHz on-chip pads. 'Probe1/In' denote the probe/microstrip side of the pad structure, respectively.

III. Marchand-like balun

A 3-D model of the 300 GHz balun with the coupled-line equivalent circuit model is shown in Fig. 2. It consists of multiple broadside-coupled asymmetric line sections with a close-proximity side ground-plane for compact realization. The line parameters are chosen non-uniformly to compensate for the frequency-dependent pad impedance. The cascaded line sections $'1\text{-}2\text{-}3'$ transform the pad impedance at port $'In'$ to some intermediate value, Z_{int1}, below the 100 Ω impedance at the balanced port, $'Out\text{-}Out'$. Z_{int2} is the impedance seen by $'1\text{-}2\text{-}3'$, which involves a 100 Ω load impedance and the one available at the output of another non-uniform line section $'3\text{-}4\text{-}5'$. $Z_{\theta 1,3,5}$ are used to control the balun imbalance.

A. Simplified analysis

An ideal planar equivalent of the compensated Marchand balun assumes that the transmission lines formed by coupled 2 strips are isolated from the ones formed by the lower conductors and the global surrounding ground. In this case, the unbalanced-to-balanced conversion is covered only by the line impedance, Z_{top}, defined by the standalone coupled strips, and the impedance of the bottom shunt strips, Z_{bot}, is connected in parallel to the balanced load, Z_l, at $Out\text{-}Out'$. This, in series connection with reactance seen at the through port of the open-circuit top conductor in $'3-4-5'$, defines the internal impedance Z_{int2}, which needs to be matched to Z_{int1} provided

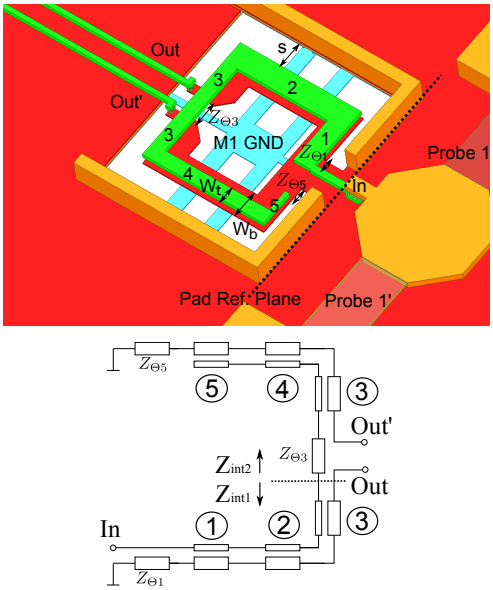

Fig. 2. Balun-integrated differential pad: (top) 3-D simulation model of the 300 GHz implementation, (bottom) simplified coupled-line model of the balun.

by $'1-2-3'$. Here, the line parameters (impedance/electrical length) of the open-stub can be further exploited for the bandwidth extending off-center balun design with 2 in-band return loss minima. The choice of both Z_{bot} and Z_{top} in relation to Z_l impacts the operation bandwidth, [2], as well as balun imbalance [3] across the bandwidth.

The balun imbalance in part originates from the phase velocity mismatch of the coupled-lines. Its partial compensation is achieved with a short line section, $Z_{\theta 3}$, at the balanced port, similarly to [4]. For broadband compensation, 2 additional degrees of freedom, $Z_{\theta 1}$ and $Z_{\theta 5}$, are further exploited (see Fig. 2). They represent an effective length difference between bottom and top strips introduced in the line sections $'1'$ and $'5'$, and as such they can be positive as well as negative. They can be viewed as additional reactive loads on the short-circuited ports of the bottom strips [5]. With asymmetry in phase velocity, the effective coupling factor, K, between the lines, as gathered in Tables 1/2, is further modified as compared to the common k_c/k_l defined from the capacitance/inductance matrix [6]. The balun is implemented with buried layers TM1 and M3 to minimize velocity mismatch between 2 normal modes which was calculated to be 5–6 %.

B. Rigorous analysis

Although perfect isolation of the coupled-lines from the close-proximity ground plane is practically unfeasible on a chip level, it is a common practice to apply this condition in the design process. Here, we demonstrate that the well-balanced balun can be designed including the impact of a global ground. For that purpose, we use a general modal analysis of the asymmetric coupled-lines in inhomogeneous medium [7], [8] with 2 normal modes, known as $'c'$ and $'\pi'$. With reference to Fig. 2, the corresponding modal impedances, $Z_{c,t}$, $Z_{\pi,t}$ and $Z_{c,b}$, $Z_{\pi,b}$, can be defined for the top and the bottom strip, respectively, in each coupled-line section numbered from $'1'$ to $'5'$. Both modes correspond to a linear combination of voltages on the top and the bottom strip under certain magnitude/phase relations, as given by the voltage ratios R_c and R_π. It can be further shown that the following holds: $Z_{c,t}/Z_{c,b}$=$Z_{\pi,t}/Z_{\pi,b}$=$-R_cR_\pi$. From the network model point of view, a single coupled-line section can be represented by a 4×4 Z-matrix [7], whereby each entry in the matrix is a linear superposition of 2 terms, each depending on either $'c'$ or $'\pi'$ mode. Provided that an ideal perfectly balanced balun can be considered a suitable connection of 2 coupled-line sections with a center tap of the top strip at the balanced output terminated with an ac short, the general 4-port coupled-line model can be reduced to 2 ports. Assuming further for simplicity that the propagation constants, γ_c and γ_π, for both modes are equal, and the effective line length is around $\lambda/4$, the coupled-line acts as an impedance transformer providing an ideal match at its both ports, with the following satisfied:

$$Z_{eff} = \sqrt{Z_l \cdot Z_g} = \frac{ab \cdot (R_c - R_\pi)^2}{a \cdot R_c + b \cdot R_\pi} \tag{1}$$

$$a = \frac{Z_{c,b}}{1 - R_c/R_\pi} \qquad b = \frac{Z_{\pi,b}}{1 - R_\pi/R_c} \tag{2}$$

Z_g/Z_l denote the termination impedances at the input/output ports, whereas Z_{eff} stands for the effective transforming impedance of the coupled-line section. It can be noticed that Z_{eff} involves not only the modal impedances but also R_c/R_π.

R_π=∞/R_c=1 corresponds to an ideal Marchand balun perfectly isolated from a global ground. Here, the simplified analysis from the previous section can be applied. However, any realistic on-chip balun implementation should account for the ground-proximity effects. Its accurate circuit representation [8] becomes more involved and should include a number of R_c/R_π transformers accounting for coupling between 2 non-identical strips in each line section. In particular, the short-circuited bottom strips do not only act as shunt stubs at the balanced output but also contribute to the overall impedance transformation along $'1$-2-$3'$ and $'3$-4-$5'$. The previously defined Z_{eff} can be used for initial dimensioning of the coupled-line sections before full-wave optimization.

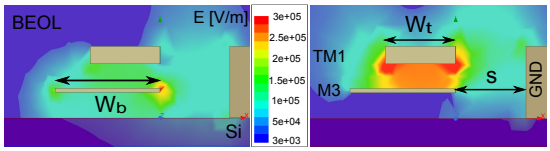

Fig. 3. E-field distribution of a coupled-line in: (left) c-mode, (right) π-mode.

IV. Balun-integrated differential pad

All major dimensions for each buried line section in the 300 GHz balun model from Fig. 2 with the corresponding modal parameters are gathered in Table 1. Z_{eff} of each sub-$\lambda/4$ long ('$\theta_{0.3THz}$') line section varies nonuniformly in view of the frequency-dependent pad impedance. The line modal parameters were extracted from the 2-D quasi-static

simulations (Ansys 2D Extractor) of a general multi-conductor system. One exemplarily chosen cross-section with the E-field distribution at 300 GHz for the $'c/\pi'$ modes is shown in Fig. 3.

All line sections are operated in the proximity of the critical point [6]; with $k_c \approx k_l$ and the voltage vectors R_c, R_π in-phase. Considering that $Z_{c,t}/Z_{c,b}=Z_{\pi,t}/Z_{\pi,b}=-R_cR_\pi$, it implies that some modal impedances become negative. These are $Z_{c,t}$ and $Z_{\pi,b}$ in our case. The $Z_{c,b}$ and $Z_{\pi,t}$ are positive and are listed in Table 1. All parameters are, in general, complex numbers due to the presence of losses, and only their magnitudes are given for simplicity. The total electrical lengths of $'$1-2-3$'$ and $'$3-4-5$'$ are different from each other; both below $\lambda/4$ at 300 GHz. Z_{eff} non-uniformly distributed along $'$1-2-3$'$ transforms the pad impedance to around 70–80 Ω (Z_{int1}) which is further matched to the balanced 100 Ω load.

Table 1. Dimensional/modal parameters of coupled lines in the 300 GHz balun

Sec.	w_t/w_b/s [μm]	K –	$\theta_{0.3THz}$ [deg]	$\lvert R_c\rvert/\lvert R_\pi\rvert$ –	$\lvert Z_{c,b}\rvert/\lvert Z_{\pi,t}\rvert$ [Ω]	$\lvert Z_{eff}\rvert$ [Ω]
1	8/12/8	0.7	19.5	0.61/3.8	57/46	47
2	10/12/11	0.77	36.5	0.65/3	59/46	41
3	6/12/10	0.69	15.5	0.62/3.92	62/53	56
4	6/12/12	0.72	38	0.63/3.63	64/54	53
5	2/12/8	0.56	10	0.55/5.85	64/71	90

The effective lengths of the imbalance-compensating line sections $Z_{\theta 1}$, $Z_{\theta 3}$, and $Z_{\theta 5}$, as defined in Sec. III-A, are -6 μm, 9 μm, and 6.5 μm, respectively. An appropriately patterned gnd plane on M1 inserted under the balun layout minimizes the leakage of parasitic CM signals to the substrate. The simulated S-parameters of the pad-loaded 300 GHz balun against the nominal 50–100 Ω design are plotted in Fig. 4. The 10-dB operation bandwidth is reduced from 180–430 GHz to 190–360 GHz due to the higher impedance transformation between the unbalanced and balanced ports. A trade-off between a fractional operation bandwidth and an in-band return loss as a function of the open-ended line length section $'$5$'$ is presented in Fig. 5. The simulated conversion to common-mode vs. the lengths of $Z_{\Theta 1}$ and $Z_{\Theta 5}$ is shown in Fig. 6. The simulated values correspond to the amplitude and phase imbalance of 1.035 and 1.6°, respectively, at maximum across 140–360 GHz. From Figs. 5, 6, it can be further noticed that conversion is largely independent from the length of $'$5$'$ whereas RL only weakly depends on the $Z_{\Theta 1}/Z_{\Theta 5}$ lengths, which allows independent tuning of both balun parameters.

The line parameters with the corresponding simulations for the pad-compensating balun operating at 60-150 GHz are gathered in Table 2 and Fig. 7. Here, in view of the lower requested transformation ratio, the reduction of a fractional bandwidth referring to the nominal 50–100 Ω design is lower. In comparison to the 300 GHz design, the impedance profile, Z_{eff}, along the line sections $'$1-2-3$'$ and $'$3-4-5$'$ is different. In particular, the aim of $'$1$'$ is to absorb the pad capacitance.

The measurements were performed after the initial TRL calibration on a standard calibration substrate with a set of

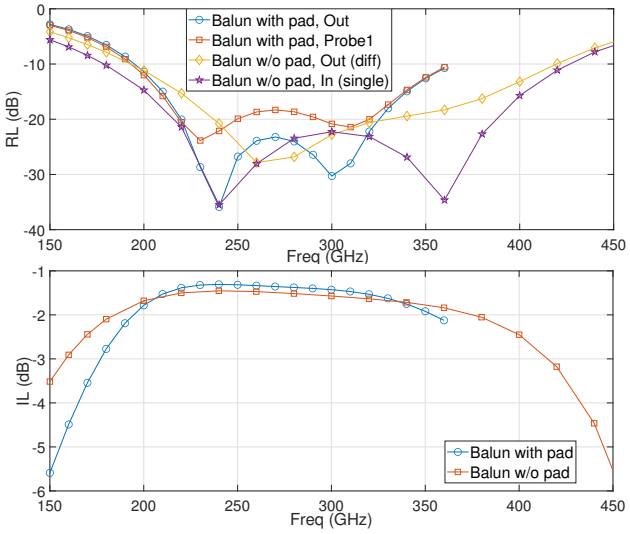

Fig. 4. Simulated RL/IL of the pad-integrated 300 GHz balun and of the nominal 50–100 Ω balun without pad. For port definition, refer to Fig. 2.

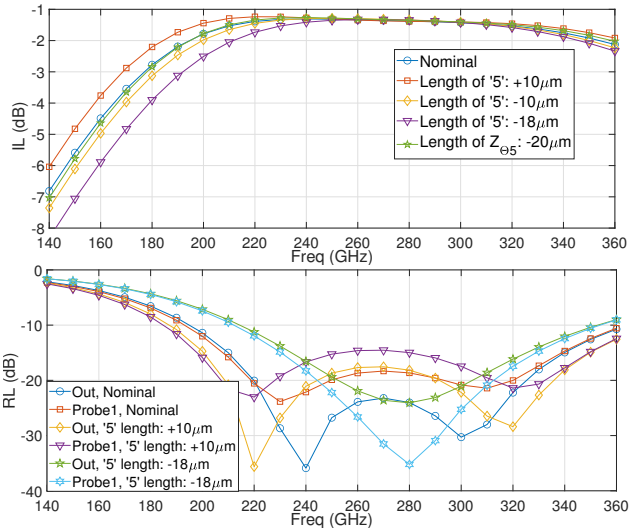

Fig. 5. Simulated RL/IL of the pad-integrated 300 GHz balun vs. the length change in the section '5'. Sensitivity to the length variation of $Z_{\Theta 5}$ is low.

extension modules from RPG/OML covering the WR10, WR6, and WR3 frequency bands. Due to the missing equipment for WR5 /WR2.2, the simulated performance could not be verified completely. In view of the challenges related to accurate characterization of the balanced ports operating at

Table 2. Dimensional/modal parameters of coupled lines in the 100 GHz balun

Sec.	w_t/w_b/s [μm]	K –	$\theta_{0.1THz}$ [deg]	$\lvert R_c\rvert/\lvert R_\pi\rvert$ –	$\lvert Z_{c,b}\rvert/\lvert Z_{\pi,t}\rvert$ [Ω]	$\lvert Z_{eff}\rvert$ [Ω]
1	2/12/8	0.61	17	0.52/4.66	63/71	90
2	4/12/11	0.71	41	0.58/3.41	65/67	67
3	5/12/10	0.71	15	0.57/3.38	61/61	62
4	7/12/11	0.76	40	0.62/2.92	60/54	49
5	6/12/8	0.7	14	0.57/3.53	56/55	57

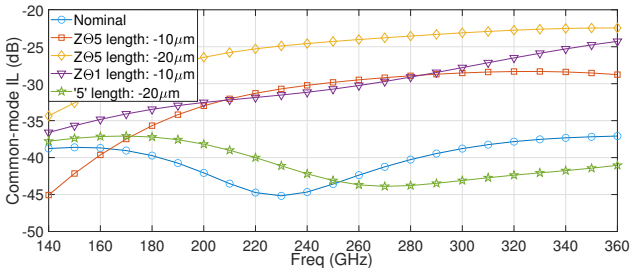

Fig. 6. Simulated parasitic conversion to the common-mode of the pad-integrated 300 GHz balun vs. the length change in the line sections $Z_{\Theta 5}$ and $Z_{\Theta 1}$. The sensitivity to the length variation of '5' is low.

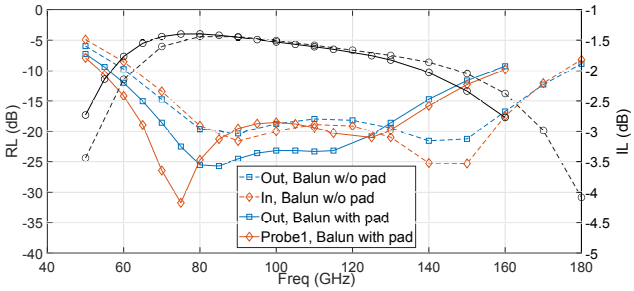

Fig. 7. Simulated RL/IL of the pad-integrated 100 GHz balun (solid) and the nominal 50–100 Ω balun w/o pad (dashed). For port definition, refer to Fig. 2.

100–300 GHz, the baluns were arranged into a back-to-back configuration with 2 different lengths of 100 Ω differential lines in between, as shown in Fig. 8. The length difference corresponds to around $\lambda/4$ in the passband to establish a constructive/destructive reflection scenario at the internal balanced ports. Only with the near-ideal load conditions (mismatch) and low CM conversion at the internal nodes, the overall RL/IL for both lengths allows indirect performance verification of a single standalone balun by simple correlation with the simulations. The measured and simulated results correspond well to each other, although by comparison to the simulations, some discrepancy in the anticipated physical material parameters seems to be observed. In view of the broadband operation with low RL, an in-band insertion loss of the single balun-integrated pad can be de-embedded from the back-to-back arrangement with a short line length ('sh'). It is 1.3–1.5 dB and 1.25–2.15 dB for the 300 GHz and 100 GHz baluns, respectively.

V. Conclusion

A set of balun-integrated 100/300 GHz differential on-chip pads was presented. A general analysis of asymmetric coupled-lines was used to design a nonuniformly-sized Marchand balun with a close-proximity gnd plane to compensate for the frequency-dependent pad impedance. Thanks to their broadband operation with low return loss, the balun-integrated pads can be used for full/multi-band small/large-signal characterization of active circuits with simple 2nd-tier on-chip transmission calibration, accounting for the balun loss, after the initial full 2-port calibration with a standard calibration substrate.

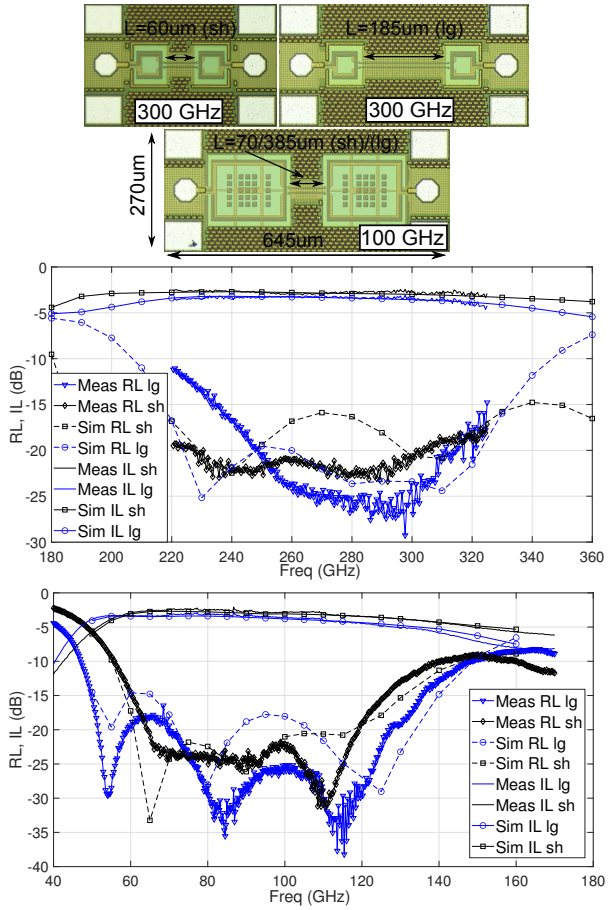

Fig. 8. Implemented 300/100 GHz baluns in a back-to-back configuration with 2 different line lengths ('sh'/'lg') in between: micrographs (top), simulated vs. measured RL/IL for the 300 GHz (middle) and 100 GHz (bottom) designs. The corresponding 'sh'/'lg' are 60/185 μm and 70/385 μm long, respectively.

References

[1] M. Wojnowski, V. Issakov, G. Sommer, and R. Weigel, "Multimode TRL Calibration Technique for Characterization of Differential Devices," *IEEE Trans. Microw. Theory Tech.*, vol. 60, no. 7, pp. 2220–2247, July 2012.

[2] H. K. Chiou and T.-Y. Yang, "Low-Loss Broadband Asymmetric Broadside-Coupled Balun for Mixer Design in 0.18-um CMOS Technology," *IEEE Trans. Microw. Theory Tech.*, vol. 56, no. 4, pp. 835–848, April 2008.

[3] S. Daneshgar and J. F. Buckwalter, "Compact Series Power Combining Using Subquarter-Wavelength Baluns in Silicon Germanium at 120 GHz," *IEEE Trans. Microw. Theory Tech.*, vol. 66, no. 11, pp. 4844–4859, 2018.

[4] M. Hossein et al., "A Compact Broadband Marchand Balun for Millimeter-Wave and Sub-THz Applications," in *GeMiC 2020*, Cottbus, Germany, March 2020, pp. 60–62.

[5] R. Ravee et al., "Inductively Compensated Parallel Coupled Microstrip Lines and Their Applications," *IEEE Trans. Microw. Theory Tech.*, vol. 54, no. 9, pp. 3571–3582, Sep. 2006.

[6] K. Sachse, "The Scattering Paramters and Directional Coupler Analysis of Characteristically Terminated Asymmetric Coupled Transmission Lines in an Inhomogneous Medium," *IEEE Trans. Microw. Theory Tech.*, vol. 38, no. 4, pp. 417–425–739, April 1990.

[7] V. K. Tripathi, "Asymmetric Coupled Transmission Lines in an Inhomogeneous Medium," *IEEE Trans. Microw. Theory Tech.*, vol. 23, no. 9, pp. 734–739, Sep. 1975.

[8] C.-M. Tsai and K. C. Gupta, "A Generelized Model for Coupled Lines and its Applications to Two-Layer Planar Circuits," *IEEE Trans. Microw. Theory Tech.*, vol. 42, no. 12, pp. 2190–2199, Dec. 1992.